Electrochemical Studies of Water-Soluble Palladium Nanoparticles

Shaowei Chen[1, 2] and Kui Huang[1]

Aqueous-soluble monolayer-protected palladium nanoparticles were synthesized by hydrogen reduction of Pd(II) in a water solution. The particles were then further functionalized by incorporating multiple copies of mercapto derivatives of viologen into the particle protecting monolayers. The electrochemistry of the viologen moieties with the particles dissolved in solution or immobilized onto electrode surfaces was carefully studied using various electrochemical techniques. The particle molecular capacitance was evaluated by rotating-disk-electrode voltammetry and the electron-transfer rate constant of the particle-bound viologen moieties was estimated by impedance measurements.

INTRODUCTION

There have been extensive research efforts directed toward the fabrication and manipulation of nanoscale advanced materials, in part, because of their unique characteristics that bridge those of the single molecules and bulk materials [1, 2]. Among these, monolayer-protected nanoclusters (MPCs) [3–6] have attracted particular attention, in that these particles behave as jumbo artificial molecules and they are stable in both solution and dry forms, in sharp contrast to conventional "naked" colloidal particles [1d]. Understandably, the MPC molecular properties can be readily manipulated by both the specific structures of the protecting monolayers and the core metals as well. Surface place-exchange or couple reactions [7]

[1] Department of Chemistry, Southern Illinois University, Carbondale, Illinois 62901-4409.

[2] To whom correspondence should be addressed at Department of Chemistry and Biochemistry, Southern Illinois University, Neckers Building, Mailstop 4409, Carbondale, Illinois 62901-4409. Fax: (618) 453-6408. E-mail: schen@chem.siu.edu.

have been found to be an efficient route to introduce multiple copies and/or identities of functional groups onto the same particle core surface, leading to the possible development of multifuntional reagents. As to the core structures, it has been found that the size, shape and the specific metal elements are all important experimental parameters that can be used to tailor the nanoparticle properties [8–10]. For instance, in an attempt to expand the MPC family, previously, we described the synthesis of alkane-thiolate-protected palladium nanoparticles using a biphasic route [10].

It should be noted that earlier studies of MPC materials are confined primarily to organic media [3–7], as particle solubility is governed mainly by the terminal structures of the protecting monolayer ligands and most of the mercapto molecules available are hydrophobic, rendering the particle soluble mostly in nonaqueous solutions. However, interests in aqueous-soluble MPCs have been growing rapidly due to the fundamental importance of investigating the media effects on the particle properties as well as their possible applications in biological systems. There has been only a scattering of reports on MPC materials that are soluble in water solutions, where the particle protecting monolayers involve mainly, for instance, ω-carboxylic/ammonium groups, oligonucleotide, or oligopeptide segments [11]. In this report, we describe the synthesis of palladium nanoparticles that are protected by a self-assembled monolayer of ammonium-terminated mercapto ligands by utilizing hydrogen reduction [12] in an aqueous solution, followed by a series of spectroscopic and electrochemical characterizations.

The obtained Pd particles are very soluble in water in all pH. As an initial attempt to use the above water-soluble particles as multifunctional reagents, thiol derivatives of electroactive viologen are incorporated into the particle protecting monolayer using surface place-exchange reactions, where the corresponding electrochemical responses from the viologen moieties are carefully examined with the particle in solutions and immobilized onto electrode surfaces. The discrepancy from those of viologen monomers is discussed. Technical implications, for instance, in the application as electron-transfer mediators are also presented.

EXPERIMENTAL

Materials. Palladium chloride ($PdCl_2$; 96%; ACROS), hydrochloric acid (HCl; Fisher), 1,9-nonanedithiol (HSC9SH; 95%; Aldrich), and all solvents (Fisher) were used as received. Water was supplied with a Barnstead Nanopure water system (18.3 MΩ). N,N,N-Trimethyl(8-mercaptooctyl)ammonium chloride (TMMAC) [13] and N-methyl-N'-(10-mercaptodecyl) viologen dihexafluorophosphate [$MMDV^{2+}(PF_6^-)_2$] [14] were synthesized and purified by adopting separate literature procedures.

Particle Synthesis.   Aqueous-soluble palladium nanoparticles protected by a monolayer of TMMAC was synthesized by H_2 reduction of Pd(II) in a water solution [12]. Specifically, 0.17 g (1 mmol) of $PdCl_2$ was first dissolved in 50 ml of 0.5 M HCl under vigorous stirring, to which 0.24 g of TMMAC (~ 1 mmol) was subsequently added. The palladium nanoparticles were then synthesized by passing hydrogen into the solution, where the solution color was found to change from orange/red to dark green/ black after ca. 10 min of reduction. The reaction appeared to be completed in about 30 min. Purification of the palladium nanoparticles was effected by dialysis where the solution was transferred to a 6-in. segment of cellular ester membrane tubing (Spectra/Por CE; MWCO = 10,000), placed in a 2-L beaker of Nanopure water, and stirred slowly. The water was recharged about every 24 h over a period of 96 h. The particles were then collected from the dialysis tube and the solvent was removed under reduced pressure with a rotary evaporator at $<40°C$. The sample was found to be spectroscopically clean by ^1H NMR measurements, free of sharp features that were ascribed to free thiol ligands and reaction by-products. The particles were found to be very soluble in water, but not in organic media (such as alcohols, acetone, alkanes, etc.).

Viologen-derivatized particles were obtained by surface place-exchange reactions [7]. Experimentally, 28 mg of the above-mentioned Pd particles was dissolved in 10 ml of H_2O, and 5 mg of $MMDV^{2+}(PF_6^-)_2$ was dissolved in 10 ml of acetone. These two solutions were then mixed together and under constant stirring for about 2 days. The solvents were then removed and the particles were purified by rinsing with copious acetone to remove the excessive free thiol and displaced thiolate ligands. The final product was again subject to NMR characterization to check the cleanness. In addition, from the integrated peak areas of the terminal functional groups, the exchange extent was estimated to be about 17%.

Particle Self-Assembled Monolayers.   The self-assembling of nanoparticles onto electrode surfaces was achieved by using surface-active particle molecules, following a procedure that we developed earlier [15]. Experimentally, 10 mg of the above-obtained viologen-derivatized TMMAC-protected Pd particles was dissolved in 3 ml of nanopure water, and $\sim 0.5\,\mu l$ of 1,9-nonanedithiol was dissolved in 3 ml of acetone; these two solutions were then mixed under magnetic stirring (the initial ratio of TMMAC: HSC9SH $\approx 4:1$). The exchange reaction was run for about 24 h, and acetone was removed under reduced pressure using a rotary evaporator. Excessive 1,9-nonanedithiols were then removed by repeated extraction with hexane. A cleaned gold disk electrode (cleaning procedure similar to that described below) was then immersed in the solution and soaked for

24 h. The electrode was rinsed thoroughly with copious water to remove loosely bound ligands and particles, before being transferred to an electrolyte solution for electrochemical measurements.

Spectroscopic Measurements. The particle core size was characterized using a Hitachi H7100 transmission electron microscope, where the samples were prepared by drop-casting the aqueous solution (ca. 1 mg/ml) onto a 400-mesh Formar-coated copper grid. Microimages were acquired with at least three spots at 300 K to 400 K magnification. ^1H NMR spectroscopy was carried out with a Varian 300 VX NMR spectrometer with concentrated particle solutions in D_2O. UV–vis spectroscopy was performed with an ATI Unicam (UV4) UV–vis spectrometer with a resolution of 2 nm using a 1-cm quartz cuvette.

Electrochemical and Impedance Measurements. Electrochemical measurements were carried out under ambient conditions with a BAS 100B/W Electrochemical Workstation, which was coupled to a BAS RDE-1 rotating-disk-electrode (RDE) module. Impedance measurements were performed with an EG&G PARC 283 Potentiostat/Galvanostat and a 1025 Frequency Response Detector. Impedance spectra were fitted using a commercial program from EG&G with the proposed equivalent circuit. A gold disk sealed in glass tubing was used as the working electrode, a Ag/AgCl (3 M NaCl) as the reference, and a Pt coil as the counterelectrode. In RDE experiments, a glassy carbon electrode (diameter, 3 mm) was employed as the working electrode. Prior to use, the (working) electrodes were polished with 0.05-μm α-Al_2O_3 slurries and rinsed thoroughly with copious dilute H_2SO_4, H_2O, ethanol, and acetone, consecutively. The electrolyte solution was degassed for at least 20 min with a water-saturated N_2 stream and blanketed with a N_2 atmosphere during the entire experimental procedure.

RESULTS AND DISCUSSION

We begin the studies with some preliminary investigations of the particle core size by using transmission electrode microscopy (TEM) and the particle optical properties with UV–vis spectroscopy. Electrochemical studies of the viologen-derivatized particles are then presented, where effects of the particle double-layer charging are studied. Finally, the electron-transfer kinetics of the particle-bound viologen moieties are investigated using impedance measurements with surface-immobilized particle assemblies. Comparison with viologen monomers is also discussed.

Particle Characterizations. Transmission electron microscopy (TEM) has been used extensively to examine the size and size distribution of

nanosized particulate materials [3–12]. Figure 1 shows a representative TEM micrograph of the above-obtained palladium particles protected by a monolayer of TMMAC, while the inset depicts the particle size histogram. One can see that the particles generated are mostly spherical, which is very different from the platinum particles synthesized in a similar manner, where different shapes of the nanocrystals were found [9]. The Pd particles formed here fall mainly into the range of 4 to 6.5 nm in diameter, with five major populations, centered at 3.9, 4.6, 5.2, 5.8 and 6.5 nm, which, by assuming an octahedral core configuration, correspond approximately to 7-, 9-, 10-, 11-, and 12-shell structures, respectively. In addition, the overall *average* particle diameter is 5.05 nm (corresponding to a 10-shell structure consisting of about 3800 Pd atoms), with a dispersity of 1.00 nm ($\sim 20\%$). The dispersity is relatively small, and comparable to that of particles synthesized using the biphasic route [10], which, akin to silver nanoparticles [8], indicates that nanoparticles of metals of the fifth period are energetically rather selective. This might be ascribed partly to the relatively weak metal–metal and metal–sulfur bonding interactions compared to those of the metal elements in the sixth period (e.g., Au [3–8] and Pt [9]), where a variation of the particle structure and a wide range of particle size are more likely to be tolerated.

One of the intrinsic properties associated with nanosized particles is their characteristic optical response. In UV–vis spectroscopic measurements, typically an exponential-decay profile is observed with decreasing photon energy (the so-called Mie scattering), onto which, depending upon the specific core metal materials, sometimes a well-defined surface-plasmon resonance band is superimposed [16]. Previous studies of alkanethiolate-protected palladium nanoparticles in organic media have shown that Pd nanoparticles do not exhibit a visible surface-plasmon band [10]. Figure 2 shows the UV–vis spectra of TMMAC-protected Pd particles in water before and after $MMDV^{2+}(PF_6^-)_2$ exchange. Also shown is the absorption profile for methyl viologen monomers dissolved in water. It can be seen that these peripheral viologen moieties do not appear to affect the general absorption profile of the palladium cores. For both particles, there is only the Mie-scattering profile, with a weak and broad absorption band observed at roughly 410 nm. Previously, we also found that in organic media, relatively large particles exhibited a weak absorption band at about 410 nm [10], whereas the band at 260 nm for particles after exchange reactions is attributed to the presence of bipyridinium moieties. These observations, in addition to ^1H NMR spectroscopic measurements, further confirm the successful exchange reaction of viologen derivatives into the particle protecting monolayer.
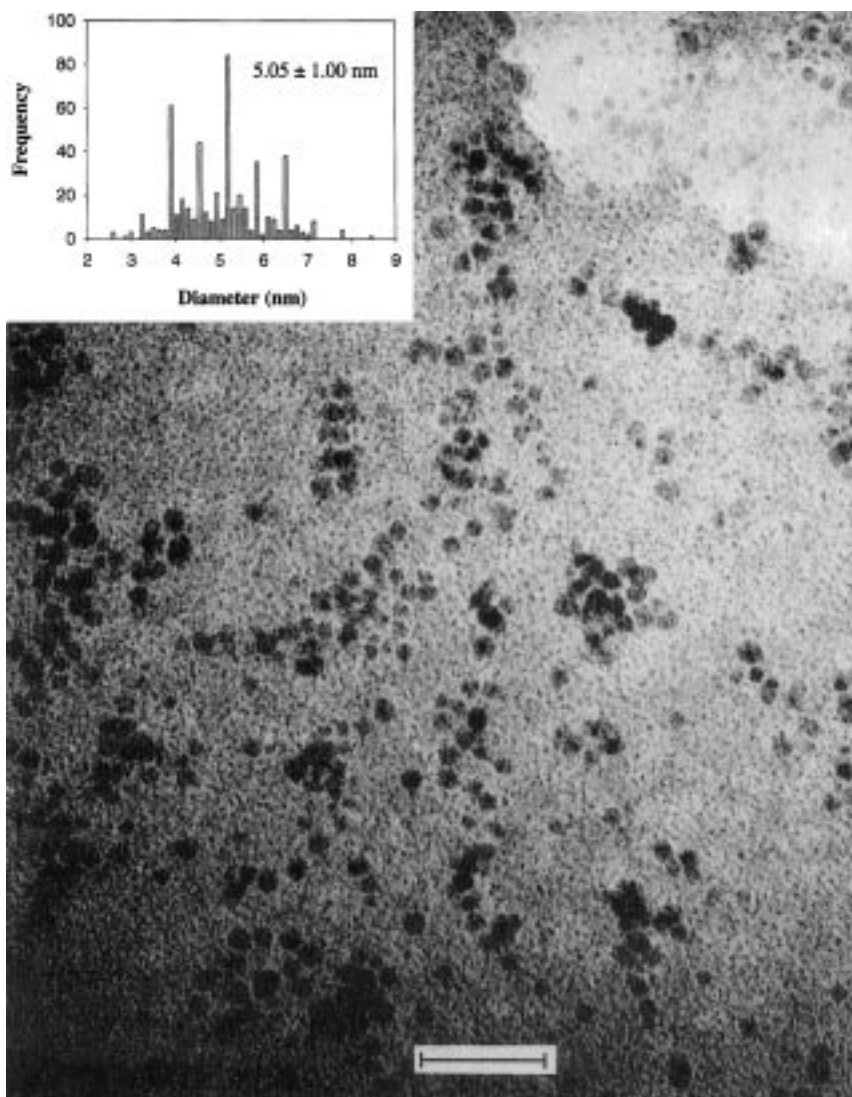
Fig. 1. Transmission electron micrograph of palladium particles protected by a monolayer of TMMAC. The scale bar is 33 nm. The inset shows the particle size histogram.
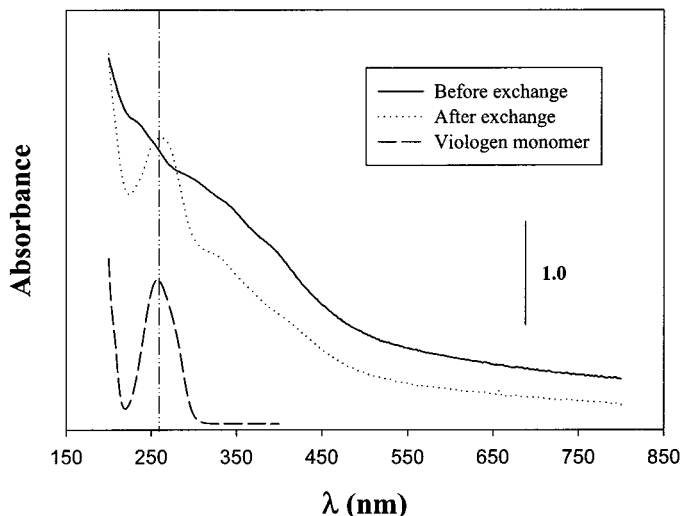
Fig. 2. UV–vis spectra of the TMMAC-protected palladium particles before and after exchange reactions with viologen mecapto derivatives $[MMDV^{2+}(PF_6^-)_2]$. Also shown is the spectrum for methyl viologen monomers. The samples were dissolved in water with a concentration in the range of 2–5 μM.

Electrochemical Measurements. Monolayer-protected nanoparticles behave as diffusive nanoelectrodes in solutions [17, 18], providing unprecedented mobile carriers for multiple copies and identities of electroactive functional groups, which might be of importance in the development of multielectron transfer mediators/catalysts [4]. It has been found that the electroactive centers residing on the same particle surface behave independently, and due to the rapid and free spinning of the particles in solution, the voltammetric current measured is the collective contribution of a series of successive electroredox reactions of these individual moieties rather than a single-step multielectron transfer reaction [18]. Figure 3A shows the cyclic voltammograms (CVs) of the viologen-derivatized Pd particles dissolved in 0.1 M NaCl at various potential sweep rates, and Fig. 3B the corresponding differential pulse voltammograms (DPVs). One can see that there are two pairs of (quasi)reversible voltammetric waves within the potential range of 0 to -1.2 V, with the formal potentials at -0.47 and -0.85 V, respectively. These two pairs of waves are attributed to the successive 1-e redox reactions involving the viologen moieties $(V^{2+} \Leftrightarrow V^{+\cdot} \Leftrightarrow V^0)$, as the peak positions are very close to those of free methyl viologens in solution $(-0.43$ and -0.81 V; not shown). Figure 3C depicts the sweep rate dependence of the peak currents, where
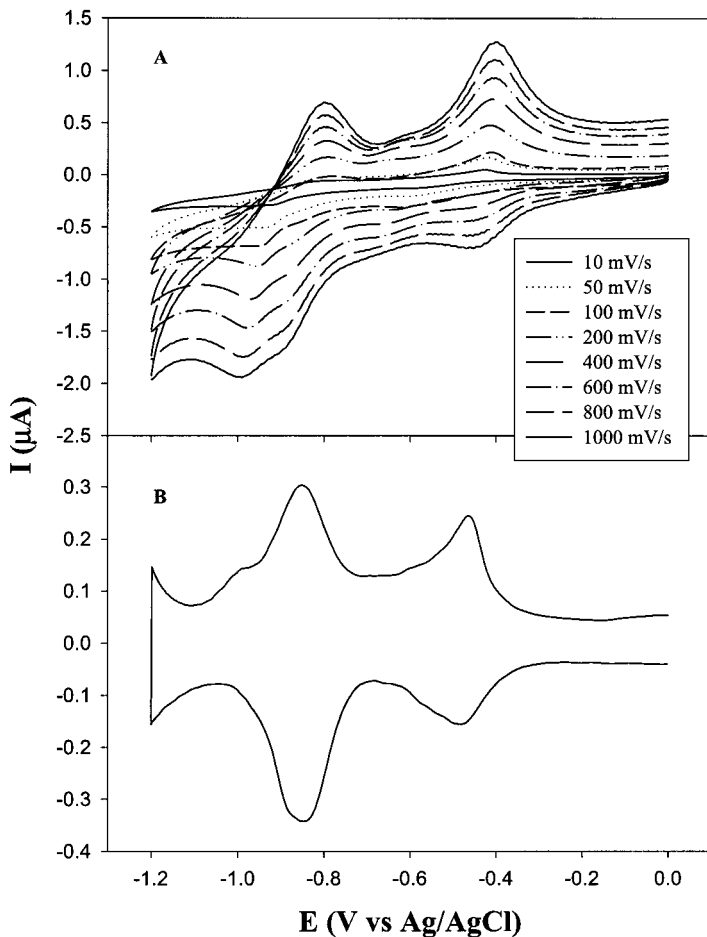
Fig. 3. (A) Cyclic and (B) differential pulse voltammograms (DPV) of viologen-derivatized TMMAC-protected Pd particles, ca. 6 μM in 0.1 M NaCl, at various potential sweep rates. Au electrode area, 0.23 mm^2. In A, the sweep rates are shown in the key, while in B the scan rate was 10 mV/s and the pulse amplitude 50 mV. (C) Variation of peak currents with the square root of potential sweep rates. Symbols are experimental data obtained from A, and lines are the corresponding linear regressions.

one can see that the peak currents are all linearly proportional to the square root of sweep rate, indicating that both waves are diffusion-controlled, i.e., the particles in solutions behave as diffusive molecules. This also implies that there was not an significant extent of particle adsorption onto the electrode surface, in contrast to gold particles, which have been
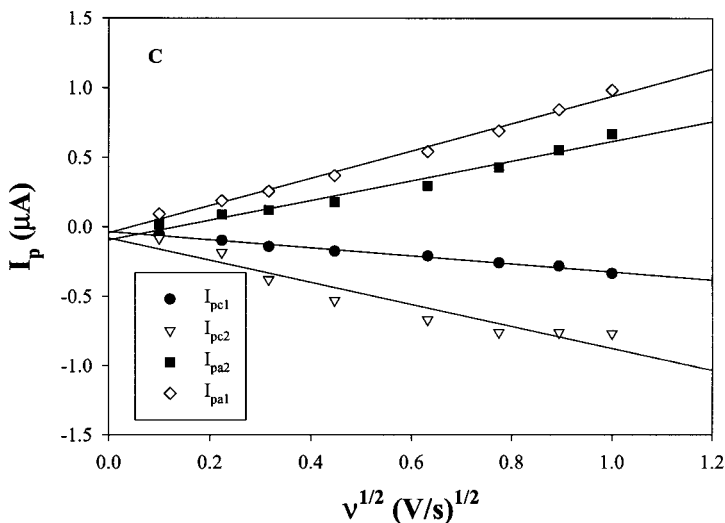
Fig. 3. *(Continued)*

found to be partially adsorbed onto the electrode surface, leading to somewhat distorted profiles [18].

On the other hand, in an earlier study [19] where the viologen-derivatized ligands were adsorbed onto a gold particle surface, the second pair of redox waves of the viologen moieties was not observed. However, it is rather unlikely that the metal core played a significant role in determining the voltammetric responses of the peripheral electroactive moieties; the discrepancy observed here is most probably due to the effectiveness of deaeration of the electrolyte solutions, as trace oxygen in the solution might affect the stability of the cationic radicals generated from the first reduction step.

To study further the electron-transfer processes involved in these voltammetric responses, we also carried out microelectrode voltammetric measurements. Figure 4A shows the voltammogram of the same particle solution at a Pt microelectrode, where two current plateaus are again very visible, with formal potentials at -0.55 and -0.80 V, respectively, slightly different from those obtained in the above CV measurements (Fig. 3). As the limiting current [20]

$$i_{\lim, c} = 4nFrDC^*\theta \tag{1}$$

where r is the electrode radius, D the MPC diffusion coefficient, C^* the MPC bulk concentration, the number of viologen moieties per MPC,
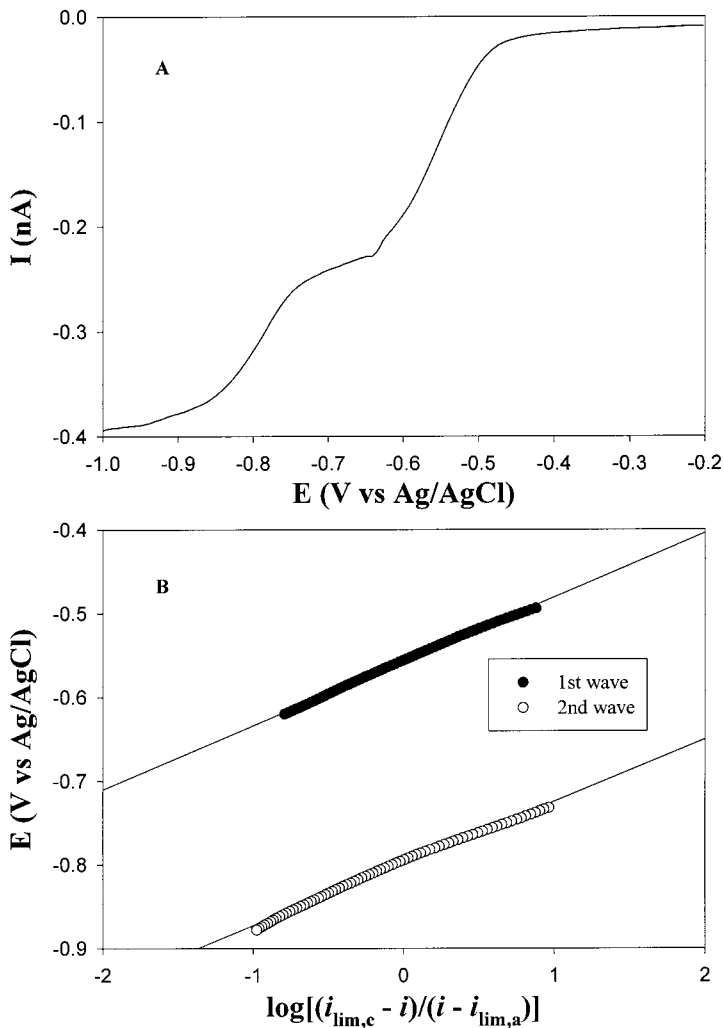
Fig. 4. (A) Voltammogram of the same Pd particle solution as in Fig. 3 at a Pt micro-electrode (diameter, $10\,\mu$m). Scan rate, 10 mV/s. (B) Waveshape analysis of the two viologen redox reactions.

and n and F have their usual significance. From Fig. 4A, one can estimate the particle diffusion coefficient to be about $3.2 \times 10^{-6}\,\text{cm}^2/\text{s}$ (here the average number of thiol ligands per particle is about 450 [12] and hence θ is about 77, as determined by NMR measurements; *vide ante*), corresponding to a hydrodynamic radius ($R_H = kT/6\pi\eta D$, where k is the Boltzmann

constant, T the solution temperature, and η the solution viscosity) of ca. 0.67 nm. This hydrodynamic radius is significantly smaller than the physical radius of the particles (~ 5 nm), and hence physically unreasonable, suggesting that the diffusion coefficient is overestimated, as part of the current might be from other sources, such as the charging of the nanoparticle double-layers [17, 18]. Similar observations were found with gold particles [19].

On the other hand, for a (quasi)reversible redox process, in the microelectrode voltammetric measurement, the current and potential have the following relationship [20]:

$$E = E_{1/2} + \frac{RT}{nF} \ln \left(\frac{i_{\lim, c} - i}{i - i_{\lim, a}} \right) \tag{2}$$

where a linear relationship is anticipated between the electrode potential (E) and $\ln[(i_{\lim, c} - i)/(i - i_{\lim, a})]$, with $i_{\lim, a}$ and $i_{\lim, c}$ being the prewave and postwave limiting currents, respectively. Figure 4B depicts the wave shape analysis for the two redox steps, both of which exhibit a slope of ~ 75 mV, somewhat greater than the 59 mV expected for a single-electron transfer process, consistent with the viologen reaction mechanism that involves two consecutive 1-e steps.

As mentioned above, these MPC molecules behave as diffusive molecular capacitors in solution, therefore, part of the current measured is attributed to the charging to the MPC double-layers. RDE voltammetry has been found to be an effective tool in estimating the molecular capacitance (C_{MPC}) of the nanoparticles [18]. Figure 5 shows the RDE voltammograms of the same Pd particle solution at various rotating rates, where one can see that the limiting current increases linearly with the square root of rotating rate (ω) (Fig. 6), again consistent with a diffusion-controlled process. In addition, the prewave and postwave current profiles are somewhat sloped, compared to those of viologen monomers (not shown), which have been ascribed to the additional contributions of the charging current to the particle double-layers [18], as observed previously with ω-ferrocenated gold nanoparticles in nonaqueous media. It has been found that the current slopes ($\Delta i/\Delta E$) are also linearly proportional to the square root of rotating rates, from which the particle molecular capacitance (C_{MPC}) can be evaluated [18]:

$$C_{\mathrm{MPC}} = (\Delta i/\Delta E)[0.62AD^{2/3}\omega^{1/2}v^{-1/6}N_A C^*]^{-1} \tag{3}$$

where A is the electrode area, v the solution kinematic viscosity, and N_A the Avogadro constant. From Fig. 6, one can estimate that the particle molecular capacitance at the prewave and postwave potentials is ~ 7.7 and
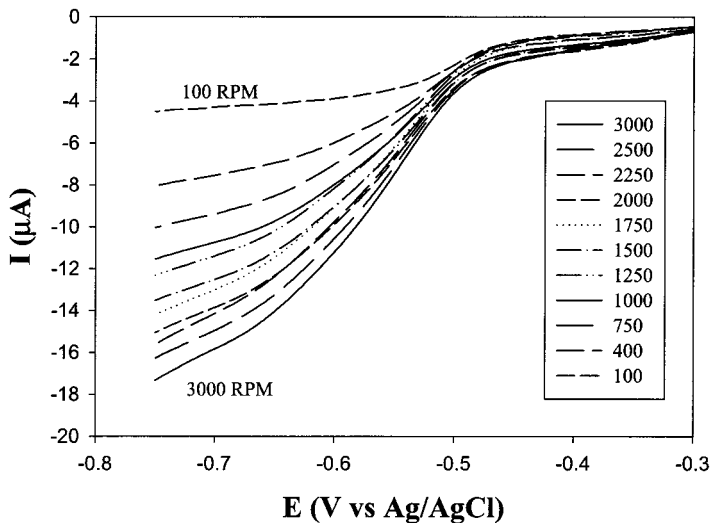
Fig. 5. Rotating-disk-electrode (RDE) voltammograms of viologen-derivatized TMMAC-protected Pd particles, ca. 4.4 μM in 0.075 M NaCl, at various rotating rates (in RPM). Glassy carbon electrode area, 0.07 cm^2. The effective concentration of viologen is about 0.34 mM.
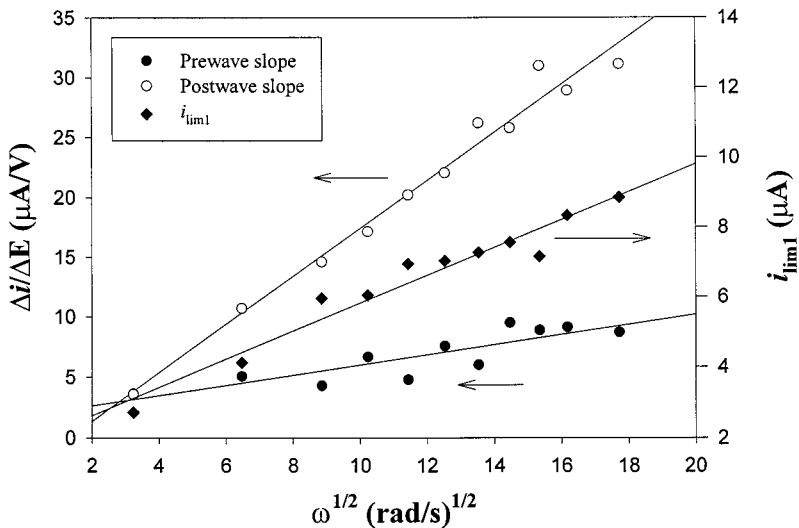
Fig. 6. Variation of limiting currents ($i_{\lim 1}$) and the prewave and postwave slopes ($\Delta i/\Delta E$) with the square root of rotating rates. Symbols are experimental data obtained from Fig. 5 and lines are the corresponding linear regressions.

37 aF, respectively. In the studies of ω-ferrocenated gold MPCs, it has also been found that the postwave MPC capacitance could be severalfold higher than the prewave one [18]. In a concentric model of the MPC structure [17c], the MPC capacitance can be expressed as

$$C_{\mathbf{MPC}} = 4\pi\varepsilon\varepsilon_0 \frac{r}{d}(r+d) \tag{4}$$

where ε is the monolayer dielectric constant, ε_0 the vacuum permitivity, r the core radius, and d the (effective) monolayer thickness. By assuming that the monolayer thickness is equal to the fully extended chain length of the thiol ligands (~ 1.25 nm), one can estimate that the (effective) dielectric constant of the MPC protecting monolayer is about 9 (before viologen reduction).

Self-Assembled Monolayers of Pd MPCs. Self-assembling of MPC molecules onto electrode surfaces can be achieved by using stable and surface-active particles [15]. In this method, the exchange reactions of the MPCs and alkanedithiols result in the incorporation of multiple copies of peripheral thiols into the MPC protecting monolayers, which can then be adsorbed onto electrode surfaces, akin to monomeric alkanethiols [15]. Here we took 1,9-nonanedithiol as the linking reagent. Figure 7A shows the cyclic voltammograms at various potential sweep rates of the above-obtained viologen-derivatized Pd particles adsorbed onto a gold electrode surface (with HSC9SH as the linkers; Scheme I), where one can see that a pair of voltammetric waves is very visible, with the formal potential at about -0.59 V, corresponding to the first 1-e redox reaction of viologens. However, this potential position is somewhat more negative than that (-0.47 V) determined in the CV measurements with particles dissolved in solution (Fig. 3). As the voltammetric current measured here is the collective contributions of all particle-bound viologen moieties, and the particles are immobilized onto the electrode surface, the energetic states of these viologen moieties are most likely to vary depending on their specific locations on the particle surface, with those farther away from the electrode surface reduced at a more negative overpotential. Therefore, the experimental formal potential might, at least in part, reflect the effective energetics of all particle-bound viologens. Previous studies [21] with surface-immobilized ω-ferrocenated Au MPCs demonstrated similar observations, and sometimes an additional pair of voltammetric waves at a more positive potential was observed, which most likely represented the additional energy barrier due to the spatial effects of the ferrocene distribution.
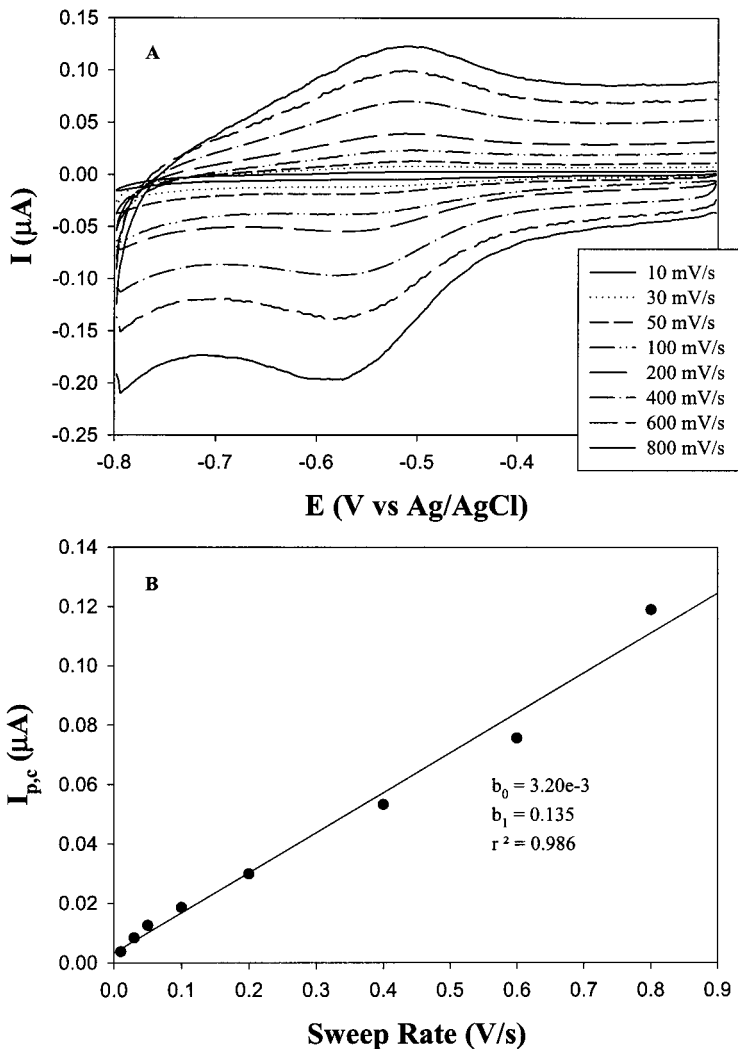
Fig. 7. (A) Cyclic voltammograms of the viologen-derivatized Pd nanoparticles self-assembled onto a gold electrode surface (2.3 mm^2) in 0.1 M NaCl at various scan rates. (B) Variation of the cathodic peak current with the sweep rate.

Figure 7B shows the variation of the voltammetric peak currents (i_p) with the potential sweep rates (v), where it can be seen that the peak current increases linearly with the sweep rate, consistent with surface-immobilized electroactive species; in addition, the slope yields a surface coverage [20] of about 6.2×10^{-12} mol/cm^2 for viologens and hence
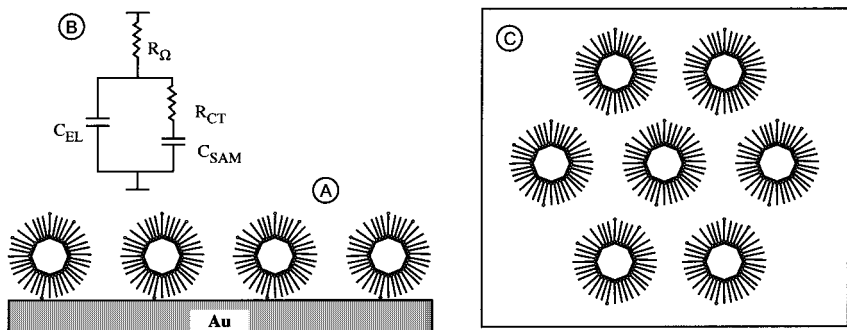
Scheme I. (A) Self-assembled monolayer of MPC molecules on an electrode surface. (B) Equivalent circuit for the surface-immobilized MPC molecules, where R_Ω is the solution resistance, R_{CT} is the charge-transfer resistance, C_{SAM} is the electrode double-layer capacitance that accounts for the part of the electrode surface with adsorbed MPCs, and C_{EL} is the electrode double-layer capacitance from the bare part of the electrode surface. (C) Hypothetical (hexagonal) structure of the MPC surface assembly.

8.0×10^{-14} mol/cm^2 for MPCs. By assuming a hexagonal structure of the surface-adsorbed MPCs (Scheme I), the effective interparticle (center-to-center) distance is about 49 nm, which is much greater than the physical diameter of the particle, ~ 8 nm (core + protecting layers). The low surface coverage might be attributed partly to the electrostatic interactions
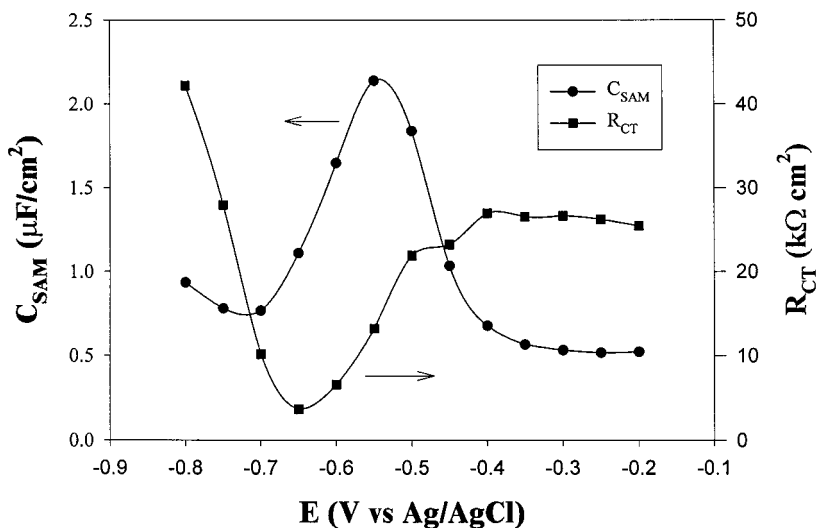
Fig. 8. Impedance measurements of the Pd MPC surface assemblies in Fig. 7. The data were obtained by fitting the impedance spectra using the equivalent circuit in Scheme I.

between positively charged particles, as well as to the dilute (ca. 6 μM) particle solution for MPC self-assembling. It is anticipated that higher surface coverage might be achieved by using more concentrated solutions.

In addition, impedance measurements were also carried out to investigate the electron-transfer kinetics of the viologen moieties of the surface-adsorbed MPCs. As mentioned above, the coverage of the MPC surface assemblies is less than a full monolayer, i.e., part of the electrode surface is covered by MPCs, while the other part is bare, and their corresponding interfacial capacitance can be represented by two separate components, C_{SAM} and C_{EL} (Scheme I), respectively (hence the overall electrode double-layer capacitance, $C_{DL} = C_{SAM} + C_{EL}$ [15]). Figure 8 shows the variation of C_{SAM} and R_{CT} (charge-transfer resistance) with the electrode potential, determined from the fitting of the impedance spectra with the equivalent circuit proposed in Scheme I, where one can see that at potentials close to the formal potential, the capacitance reaches a maximum while the charge-transfer resistance reaches a minimum. As the electron-transfer rate constant (k_{et}) of surface-immobilized electroactive moieties can be expressed as [22]

$$k_{et} = \frac{1}{2C_{SAM}R_{CT}} \tag{5}$$

from Fig. 8, one can estimate that the k_{et} for the particle-bound viologens is approximately $1.2 \times 10^3 \, s^{-1}$. This value is comparable to that obtained from similar measurements with a $MMDV^{2+}(PF_6^-)_2$ self-assembled monolayer on a gold electrode surface [23].

Viologens have been used rather extensively as electron-transfer mediators [24], thus, the above-obtained viologen-MPC surface assemblies might provide a nanoscale patterned surface structure where surface electron-transfer processes might be manipulated for sensing applications. Research to this end is in progress and results will be reported in due course.

CONCLUDING REMARKS

Aqueous-soluble palladium nanoparticles were synthesized and characterized using a variety of spectroscopic and electrochemical techniques. Multiple copies of the viologen moieties were incorporated into the particle protecting monolayers using surface place-exchange reactions. It was found that the electrochemistry of the particle-bound viologens was consistent with that of viologen monomers, with two pairs of voltammetric waves corresponding to the two consecutive 1-e redox reactions. When the viologen-derivatized Pd particles were immobilized onto the electrode

surface, the first 1-*e* redox step was observed at a more negative potential than that with the particles dissolved in solution. This was attributed partly to the spatial effect of the viologens residing on the particle surface. From impedance measurements, the electron-transfer rate constant was evaluated, which was comparable to that obtained with two-dimensional self-assembled monolayers of viologen monomers.

ACKNOWLEDGMENTS

REFERENCES

1. (a) G. Schmid, *Clusters and Colloids: From Theory to Applications* (VCH, New York, 1994). (b) H. Haberland (ed.), *Clusters of Atoms and Molecules* (Springer-Verlag, New York, 1994). (c) R. Turton, *The Quantum Dot: A Journey into the Future of Microelectronics* (Oxford University Press, New York, 1995). (d) M. A. Hayat (ed.), *Colloidal Gold: Principles, Methods, and Applications, Vol. 1* (Academic Press, New York, 1989).
2. See also all the review articles in the February 16, 1996, issue of *Science*.
3. M. Brust, M. Walker, D. Bethell, D. J. Schiffrin, and M. Whyman (1994). *J. Chem. Soc. Chem. Commun.* 801.
4. A. C. Templeton, W. P. Wuelfing, and R. W. Murray (2000). *Acc. Chem. Res.* **33**, 27, and references cited therein.
5. R. L. Whetten, M. N. Shafigullin, J. T. Khoury, T. G. Schaaff, I. Vezmar, M. M. Alvarez, and A. Wilkinson (1999). *Acc. Chem. Res.* **32**, 397, and references cited therein.
6. D. V. Leff, P. C. Ohara, J. R. Heath, and W. M. Gelbert (1995). *J. Phys. Chem.* **99**, 7036.
7. (a) A. C. Templeton, M. J. Hostetler, E. K. Warmoth, S. Chen, C. M. Hartshorn, V. M. Krishnamurthy, M. D. E. Forbes, and R. W. Murray (1998). *J. Am. Chem. Soc.* **120**, 4845. (b) A. C. Templeton, M. J. Hostetler, and R. W. Murray (1999). *Langmuir* **15**, 3782.
8. (a) C. P. Collier, R. J. Saykally, J. J. Shiang, S. E. Henrichs, and J. R. Heath (1997). *Science* **277**, 1978. (b) S. A. Harfenist, Z. L. Wang, M. M. Alvarez, I. Vezmar, and R. L. Whetten (1996). *J. Phys. Chem.* **100**, 13904.
9. T. S. Ahmadi, Z. L. Wang, T. C. Green, A. Henglein, and M. A. El-Sayed (1996). *Science* **272**, 1924.
10. S. Chen, K. Huang, and J. A. Stearns (2000). *Chem. Mater* **12**, 540.
11. (a) A. C. Templeton, S. Chen, S. M. Gross, and R. W. Murray (1999). *Langmuir* **15**, 66. (b) T. G. Schaaff, G. Knight, M. N. Shafigullin, R. F. Borkman, and R. L. Whetten (1998). *J. Phys. Chem. B* **102**, 10643. (c) M. T. Reetz and M. G. Koch (1999). *J. Am. Chem. Soc.* **121**, 7933.
12. (a) G. Schmid, M. Harms, J.-O. Malm, J.-O. Bovin, J. van Ruitenbeek, H. W. Zandbergen, and W. T. Fu (1993). *J. Am. Chem. Soc.* **115**, 2046. (b) G. Schmid (1992). *Chem. Rev.* **92**, 1709. (c) G. Schmid (1988). *Polyhedron* **7**, 2321.
13. J. Tien, A. Terfort, and G. M. Whitesides (1997). *Langmuir* **13**, 5349.
14. X. Tang, T. W. Schneider, J. W. Walker, and D. A. Buttry (1996). *Langmuir* **12**, 5921.

15. S. Chen (2000). *J. Phys. Chem. B* **104**, 663.
16. J. A. Creighton and D. G. Eadon (1991). *J. Chem. Soc. Faraday Trans.* **87**, 3881.
17. (a) R. S. Ingram, M. J. Hostetler, R. W. Murray, T. G. Schaaff, J. Khoury, R. L. Whetten, T. P. Bigioni, D. K. Guthrie, and P. N. First (1997). *J. Am. Chem. Soc.* **119**, 9279. (b) S. Chen, R. S. Ingram, M. J. Hostetler, J. J. Pietron, R. W. Murray, T. G. Schaaff, J. T. Khoury, M. M. Alvrez, and R. L. Whetten (1998). *Science* **280**, 2098. (c) S. Chen, R. W. Murray, and S. W. Feldberg (1998). *J. Phys. Chem. B* **102**, 9898. (d) J. F. Hicks, A. C. Templeton, S. Chen, K. M. Sheran, R. Jasti, R. W. Murray, J. Debord, T. G. Schaaff, and R. L. Whetten (1999). *Anal. Chem.* **71**, 3703.
18. (a) S. J. Green, J. J. Stokes, M. J. Hostetler, J. J. Pietron, and R. W. Murray (1997). *J. Phys. Chem. B* **101**, 2663. (b) S. J. Green, J. J. Pietron, J. J. Stokes, M. J. Hostetler, H. Vu, W. P. Wuelfing, and R. W. Murray (1998). *Langmuir* **14**, 5612.
19. A. C. Templeton, D. E. Cliffel, and R. W. Murray (1999). *J. Am. Chem. Soc.* **121**, 7081.
20. A. J. Bard and L. R. Faulkner, *Electrochemical Methods: Fundamentals and Applications* (John Wiley & Sons, New York, 1980).
21. S. Chen, K. M. Sheran, and R. W. Murray, unpublished results.
22. (a) S. E. Creager and T. T. Wooster (1998). *Anal. Chem.* **70**, 4257. (b) K. Weber, L. Hockett, and S. E. Creager (1997). *J. Phys. Chem. B* **101**, 8286.
23. K. Huang and S. Chen, unpublished results.
24. (a) M. Ito and T. Kuwana (1971). *J. Electroanal. Chem.* **32**, 415. (b) P. Y. Szentrimay and T. Kuwana, *in* D. Swayer (ed.), *Electrochemical Studies of Biological Systems* (American Chemical Society, Washington, DC, 1977), p. 143. (c) R. Herrero, M. R. Moncelli, L. Becucci, and R. Guidelli (1997). *J. Phys. Chem. B* **101**, 2815. (d) H. Tatsumi, K. Takagi, M. Fujita, K. Kano, and T. Ikeda (1999). *Anal. Chem.* **71**, 1753.